The binuclear cluster of [FeFe] hydrogenase is formed with sulfur donated by cysteine of an $[Fe(Cys)(CO)_2(CN)]$ organometallic precursor

Guodong Rao[a,1], Scott A. Pattenaude[b,1], Katherine Alwan[c], Ninian J. Blackburn[c], R. David Britt[a,2], and Thomas B. Rauchfuss[b,2]

[a]Department of Chemistry, University of California, Davis, CA 95616; [b]School of Chemical Sciences, University of Illinois at Urbana–Champaign, Urbana, IL 61801; and [c]Department of Chemical Physiology and Biochemistry, Oregon Health and Science University, Portland, OR 97239

Edited by Marcetta Y. Darensbourg, Texas A&M University–College Station, College Station, TX, and approved September 11, 2019 (received for review August 1, 2019)

The enzyme [FeFe]-hydrogenase (HydA1) contains a unique 6-iron cofactor, the H-cluster, that has unusual ligands to an Fe–Fe binuclear subcluster: CN^-, CO, and an azadithiolate (adt) ligand that provides 2 S bridges between the 2 Fe atoms. In cells, the H-cluster is assembled by a collection of 3 maturases: HydE and HydF, whose roles aren't fully understood, and HydG, which has been shown to construct a $[Fe(Cys)(CO)_2(CN)]$ organometallic precursor to the binuclear cluster. Here, we report the in vitro assembly of the H-cluster in the absence of HydG, which is functionally replaced by adding a synthetic $[Fe(Cys)(CO)_2(CN)]$ carrier in the maturation reaction. The synthetic carrier and the HydG-generated analog exhibit similar infrared spectra. The carrier allows HydG-free maturation to HydA1, whose activity matches that of the native enzyme. Maturation with ^{13}CN-containing carrier affords ^{13}CN-labeled enzyme as verified by electron paramagnetic resonance (EPR)/electron nuclear double-resonance spectra. This synthetic surrogate approach complements existing biochemical strategies and greatly facilitates the understanding of pathways involved in the assembly of the H-cluster. As an immediate demonstration, we clarify that Cys is not the source of the carbon and nitrogen atoms in the adt ligand using pulse EPR to target the magnetic couplings introduced via a $^{13}C_3$,^{15}N-Cys–labeled synthetic carrier. Parallel mass-spectrometry experiments show that the Cys backbone is converted to pyruvate, consistent with a cysteine role in donating S in forming the adt bridge. This mechanistic scenario is confirmed via maturation with a seleno-Cys carrier to form HydA1–Se, where the incorporation of Se was characterized by extended X-ray absorption fine structure spectroscopy.

iron carbonyl cyanides | cysteine | H-cluster biosynthesis

Hydrogenases are nature's machines for the metabolism of H_2, both its production and its oxidation. [FeFe]-hydrogenases are hyperefficient, operating at rates up to $\sim 10^4$ per second (1, 2). Investigations into [FeFe]-hydrogenases are motivated by their potential applications related to renewable energy and the design of fuel cells (3). It is therefore mandatory that we understand how nature assembles the elaborate catalytic centers at the heart of these remarkable machines.

The active site of [FeFe]-hydrogenase, the H-cluster, is a 6-Fe ensemble consisting of a canonical $[4Fe–4S]_H$ subcluster linked through a bridging Cys residue to a $[2Fe]_H$ subcluster, in which the 2 Fe ions are coordinated by distinctive cofactors: 3 CO ligands, 2 CN^- ligands, and an unprecedented azadithiolate [adt; $HN(CH_2S^-)_2$] ligand. The $[2Fe]_H$ subcluster is proposed to be the site of substrate (H^+, H_2) binding and activation (4–7). The unique structural features and catalytic activity of the H-cluster have attracted considerable interest regarding its biosynthesis, particularly of this $[2Fe]_H$ subcluster (8–14), which poses one of the greatest active-site biosynthesis challenges known for biology with multiple-component, step-by-step assembly involving toxic ligands, O_2 sensitivity, and an unusual organic bridging ligand that has little inherent stability. From low-molecular-mass precursors, the $[2Fe]_H$ subcluster is orchestrated by 3 maturases: HydE, HydF, and the multifunctional enzyme HydG. While understanding of HydE and HydF remains limited (9, 15–19), recent work has demonstrated that HydG is responsible for the biosynthesis of CN^- and CO, which are produced by degradation of tyrosine, catalyzed by a radical *S*-adenosyl-L-methionine (SAM) site (20–24). These diatomic ligands combine with a Fe(Cys) center that is bound to the auxiliary [4Fe–4S] cluster within HydG. Once assembled, this $[Fe(Cys)(CO)_2(CN)]$ module, termed "Complex B," is quickly consumed in the biosynthesis of the $[2Fe]_H$ module (the active site) of HydA1 (25–29). Due to its lability—decomposition and release of free CO occurs on the order of minutes (25)—isolated Complex B has not been tested in vitro as a precursor to the H-cluster, which, in principle, should be possible in the absence of HydG. In this paper, we report an analog of Complex B, which we call **syn-B**, which allows us to probe the biosynthesis of HydA1, leading to several important insights. We show that **syn-B** functionally replaces the proposed $[Fe(Cys)(CO)_2(CN)]$ product of HydG to generate fully active [FeFe] hydrogenase with identical spectroscopic signatures. As a robust functional surrogate of Complex B, **syn-B** allows us to carry out H-cluster assembly with isotopically labeled cysteine and with

Significance

[FeFe]-hydrogenases catalyze H_2 evolution at extraordinary rates at low overpotential using base metal (not platinum). In the field of renewable energy, the biosynthesis of these enzymes' active sites, the H-cluster, is of intense interest. Among its many cofactors, the azadithiolate is unique, and its biosynthesis remains enigmatic. Three Fe–S proteins, HydE, HydF, and HydG, are essential for the H-cluster bioassembly. This paper describes an in vitro assembly approach where a synthetic $[Fe(cysteine)(CO)_2(CN)]$ complex, "syn-B," allows HydG-free biosynthesis of the active enzyme. Using isotopic and S/Se labeling, syn-B is shown to contribute $Fe(CO)_2(CN)S$ to the biosynthesis. This work sets the stage for further investigation of the H-cluster bioassembly.

Author contributions: N.J.B., R.D.B. and T.B.R. designed research; G.R., S.A.P., and K.A. performed research; G.R., S.A.P., K.A., N.J.B., R.D.B., and T.B.R. analyzed data; and G.R., S.A.P., K.A., N.J.B., R.D.B., and T.B.R. wrote the paper.

The authors declare no competing interest.

This article is a PNAS Direct Submission.

[1]G.R. and S.A.P. contributed equally to this work.

[2]To whom correspondence may be addressed. Email: rdbritt@ucdavis.edu or rauchfuz@illinois.edu.

This article contains supporting information online at www.pnas.org/lookup/suppl/doi:10.1073/pnas.1913324116/-/DCSupplemental.

First published September 30, 2019.

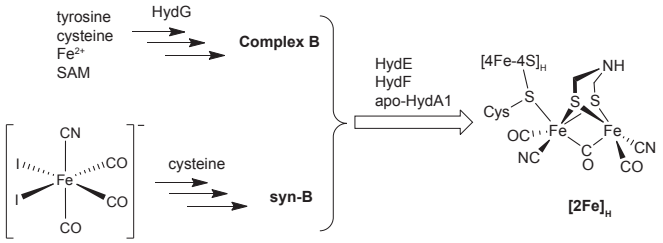

Scheme 1. Synthetic scheme showing maturation of [FeFe] hydrogenase H-cluster under normal conditions (*Upper*) and through our modular surrogate strategy (*Lower*).

selenocysteine. A combination of mass spectrometry (MS) and extended X-ray absorption fine structure (EXAFS) spectroscopy reveal that cysteine/selenocysteine donates the S/Se atoms of the adt bridge, linking the 2 Fe atoms of the binuclear cluster. Finally, experiments reveal that, while Cys serves as a source of the S in the adt, it is not the source of its central $HN(CH_2)_2$.

Results

Efforts were initially directed toward generation of Complex B by combining cysteinate salts and sources of "$Fe(CO)_2(CN)^+$." As a precursor to "$Fe(CO)_2(CN)^+$," we focused on $[FeI_2(CN)(CO)_3]^-$ (30), which we generated both by cyanation of $FeI_2(CO)_4$ or, preferably, the iodination of $[Fe(CN)(CO)_4]^-$ (31, 32). Provided that it is protected from light, the resulting $[FeI_2(CN)(CO)_3]^-$ is stable for several minutes at room temperature as a solution in methanol (see *SI Appendix*, Fig. S1 for electrospray ionization [ESI]-MS). It reacts rapidly with dipotassium cysteinate to afford a homogeneous orange solution, which upon evaporation yields a light-orange solid of **syn-B** (Scheme 1).

The Fourier transform infrared (FT-IR) spectrum of aqueous solution of **syn-B** is nearly identical to the spectrum observed for Complex B (Fig. 1), with bands at 2,107; 2,058; and 2,010 cm^{-1} [compared to 2,105; 2,057; and 2,006 cm^{-1} for natural isotopic abundance Complex B reported (25); see *SI Appendix*, Table S1 for the summary of IR bands]. The 3-band pattern is diagnostic of a facial $Fe(CO)_2(CN)$ center (33). Although they are very similar by FT-IR, **syn-B** and Complex B exhibit very different stabilities: Complex B decomposes on the order of minutes at room temperature (25), whereas **syn-B** is stable in water for hours. Additionally, **syn-B** is stable as a solid, showing no signs of decomposition after months.

ESI-MS for **syn-B** (Fig. 2 and *SI Appendix*, Fig. S2) revealed a strong peak in the negative mode at $m/z = 201.0$ corresponding to $[Fe(Cys)(CN)]^-$ (carboxylate deprotonated). The nonobservations of $[Fe(Cys)(CN)(CO)_2]^-$ is consistent with the lability of Fe^{II}-CO bonds. The assignment of the m/z 201.0 signal to $[Fe(Cys)(CN)]^-$ ion was confirmed by the preparation of several isotopologues and selenocysteine analog (vide infra; *SI Appendix*, Figs. S2–S5).

Although its formulation cannot be described precisely in the absence of X-ray crystallographic analysis, **syn-B** is a multiiron ensemble consisting of $Fe(CO)_2(CN)(Cys)$ centers bound to a high-spin ferrous iodide site. Elemental analyses (percent C, H, N, and I) are consistent with the formula $(Et_4N)_4\{FeI_2[Fe(Cys)(CN)(CO)_2(H_2O)]_4\}$, i.e., a cluster composed of 4 $[Fe(Cys)(CN)(CO)_2(H_2O)]$ centers bound to FeI_2. The ensemble exhibits a highly reproducible magnetic moment of 4.6 μ_B (calculated by Evan's method; *SI Appendix*, Fig. S6) and the presence of Et_4N^+ (observable by NMR spectroscopy). The paramagnetic ferrous center is assumed to derive from $[FeI_2(CN)(CO)_2]^-$, which is prone to decomposition. This high-spin ferrous Lewis acid provides crucial stabilization of the $Fe(Cys)(CO)_2(CN)$ fragments, analogous to the interaction of the dangler Fe and the [4Fe–4S] cluster in HydG (26, 34). Mixed-spin ferrous thiolate complexes are well precedented (35, 36).

The essential and remarkable feature of **syn-B** is that it serves as a kinetically well-behaved source of $Fe(CO)_2(CN)(Cys)$, directly applicable to the in vitro maturation of HydA1. These experiments are enumerated below.

syn-B Facilitates the Maturation of HydA1 in the Absence of HydG. The maturation of apo-*Cr*HydA1 (that harbors the $[4Fe–4S]_H$ subcluster) requires 3 maturases—HydE, HydF, and HydG—as well as various low-molecular-mass components necessary for the enzymatic reactions (37, 38). Using **syn-B**, HydG (along with its substrate, Tyr) can be omitted from this canonical recipe, leaving everything else unchanged. The electron paramagnetic resonance (EPR) spectrum of the resulting [**syn-B**]-*Cr*HydA1 poised in the thionine-oxidized state exhibits the lineshape and g values of [2.103, 2.044, 1.998] that are characteristic of *Cr*HydA1 H_{ox} (Fig. 3*A*, red traces) (1). Also present is the CO-inhibited form of the H-cluster, H_{ox}–CO, commonly seen in [FeFe]-hydrogenase samples (Fig. 3*A*, gray traces) (1).

Most importantly, [**syn-B**]-*Cr*HydA1 shows similar H_2 production activity to the standard holo-*Cr*HydA1 sample under parallel conditions (Fig. 3*B* and *SI Appendix*, Fig. S7). These results clearly indicate that **syn-B** can be used as a surrogate of the HydG reaction product to build the H-cluster. Stated more generally, **syn-B** is a fully competent precursor to the H-cluster, without the need for HydG. This result confirms the role of HydG in building $[Fe(Cys)(CO)_2(CN)]$ as an intermediate in the maturation of the hydrogenase. Furthermore, HydG-free maturation shows that direct interactions between the HydG protein and other maturation partners are not necessary for the bioassembly of the H-cluster in the cell-free system.

Maturation of apo-HydA1 with syn-B-^{13}CN Affords HydA1-^{13}CN (also in the Absence of HydG). Having established the efficacy of **syn-B** for HydG-free maturation, additional experiments were undertaken to verify the function of **syn-B**. These experiments also provided further support for its formulation. Starting from $[Fe(^{13}CN)I_2(CO)_3]^-$, we prepared the ^{13}CN-isotopologue of **syn-B**, i.e., **syn-B-^{13}CN**. The FT-IR spectrum of **syn-B-^{13}CN** and **syn-B** differ only slightly in the ν_{CO} region, showing a shift of ~11 cm^{-1} for one of the CO bands. Moreover, the ν_{CN} region was perturbed by ~33 cm^{-1} to lower energy for **syn-B-^{13}CN**, as expected (*SI Appendix*,

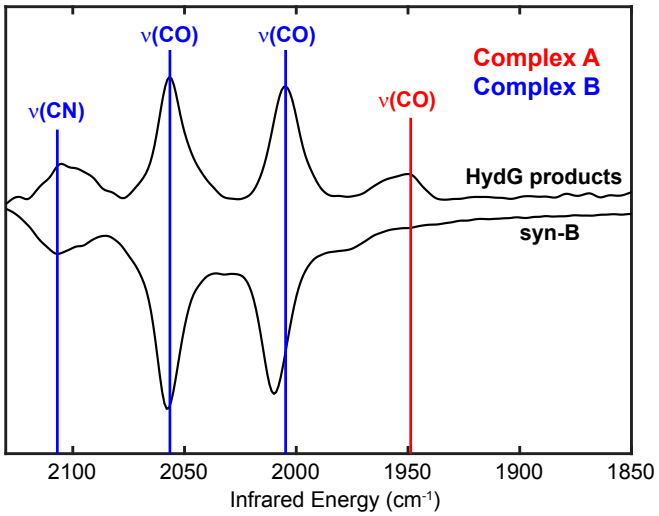

Fig. 1. FT-IR comparison of HydG reaction products observed in enzymatic reactions using Tyr as substrate (upper trace; adapted from ref. 26) and **syn-B** dissolved in H_2O (lower trace).

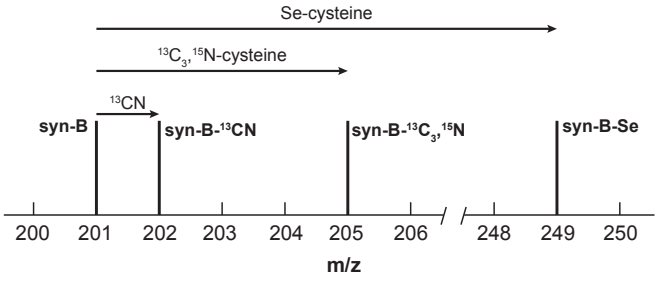

Fig. 2. Schematic representation of the effect of labeling on the parent [Fe(Cys)(CN)]$^-$ peak in the ESI-MS of **syn-B** and its analogs. Incorporation of ^{13}CN causes a shift of 1 *m/z*, the isotopologue containing $^{13}C_3$,^{15}N-cysteinate results in a shift of 4 *m/z*, and incorporation of selenocysteine (^{80}Se) causes a shift of 48 *m/z*.

Table S1). The ESI-MS of **syn-B-^{13}CN** was analogous to that for **syn-B**, except that the peak of interest assigned to [Fe(Cys)(CN)]$^-$ was shifted to 1-Da higher mass, consistent with the fragment [Fe(Cys)(^{13}CN)]$^-$ (Fig. 2 and *SI Appendix*, Fig. S3). Maturation using **syn-B-^{13}CN** generated [**syn-B-^{13}CN**]-*Cr*HydA1, the EPR spectrum of which clearly shows hyperfine splitting that has been observed in the ^{13}CN-labeled H-cluster with the ^{13}CN ligands sourced from HydG-cleaved 2-^{13}C-Tyr (39). The hyperfine interactions in [**syn-B-^{13}CN**]-*Cr*HydA1 were further probed by Q-band Davies on electron nuclear double resonance (ENDOR) spectroscopy, revealing 2 ^{13}C hyperfine values of 29.2 and 5.34 MHz at g_1 of H_{ox}, identical to those found in the ^{13}CN-labeled *Cr*HydA1 (Fig. 3*C*) (39). This result unambiguously shows that the cyanide in **syn-B** is indeed delivered into HydA1 and validates that **syn-B** is fully competent precursor to the H-cluster.

An Intact (Cys)Fe(CO)$_2$(CN) Ensemble Is Required for Maturation. The cysteamine (cysamH = $H_2NCH_2CH_2SH$) analog of **syn-B**, **syn-B-cysam**, was prepared by the reaction of Kcysam with $[FeI_2(CN)(CO)_3]^-$. The FT-IR spectrum of **syn-B-cysam** closely matched that of **syn-B**, except that the ν_{CO} bands were shifted to lower energies ($\Delta\nu_{CO} \leq 9$ cm^{-1}; *SI Appendix*, Table S1), consistent with the better electron-donation ability of cysteamine versus cysteine. Its stability is also similar to **syn-B**. The many similarities between **syn-B-cysam** and **syn-B** imply that the carboxylate remains uncoordinated in **syn-B** and probably also in Complex B.

Interestingly, replacement of **syn-B** with **syn-B-cysam** in our standard HydG-free maturation protocol did not produce holo-HydA1. This result is striking because the maturation medium contains ∼1 mM Cys; thus, the mere presence of Cys was insufficient for maturation, even in the presence of a source of "Fe(CN)(CO)$_2$." These results imply that the presence of Cys attached to the Fe(CO)$_2$(CN) moiety is essential for maturation.

The conversion of Complex B into [2Fe]$_H$ entails many steps: loss of CO, formation of a [2Fe–2SR] center, and, most remarkable of all, the generation of the adt cofactor. It is well known that adtH$_2$ and adt^{2-} are unstable (40), which implies that the cofactor is produced on an Fe$_2$ template. The 2Fe–2S clusters are well known to mediate the biosynthesis of other organosulfur cofactors (biotin and lipoic acid) (19, 41). Since L-cysteine is required for the biosynthesis of the [2Fe-2SR] center, it is thus appealing to suggest that the cysteine in Complex B, and here **syn-B**, could provide all of the ingredients (CH$_2$, NH, and S) required to assemble the adt cofactor. This Cys → adt hypothesis has not been unambiguously tested by using the reported maturation procedure, because Cys is already present in the auxiliary 5Fe–4S cluster of HydG (34), which makes labeling of Cys by adding labeled Cys exogenously inefficient. This issue can be clearly avoided by using **syn-B** as a surrogate for HydG.

Maturation of apo-HydA1 with syn-B-$^{13}C_3$,^{15}N Affords Unlabeled HydA1, i.e., Cys Is Not the Source of adt Backbone. Starting with HS^{13}CH$_2$^{13}CH(^{15}NH$_2$)^{13}CO$_2$H, we prepared an isotopologue of **syn-B**, which we call **syn-B-$^{13}C_3$,^{15}N**. The FT-IR spectra for **syn-B-$^{13}C_3$,^{15}N** and **syn-B** are virtually identical, except that the carboxylate absorbance is shifted from 1,615 to 1,575 cm^{-1}, reflecting the presence of $^{13}CO_2^-$ substituent in the heavy isotopologue. The ESI-MS of **syn-B-$^{13}C_3$,^{15}N** was also analogous to that for **syn-B**, except that the peak for [Fe(Cys)(CN)]$^-$ was shifted by 4 Da to higher mass, consistent with the fragment [Fe($^{13}C_3$,^{15}N-Cys)(CN)]$^-$ (Fig. 2 and *SI Appendix*, Fig. S4). These systematic and predictable shifts in the *m/z* values give us a high level of confidence regarding the identity of this fragment.

As expected, HydG-free maturation with **syn-B-$^{13}C_3$,^{15}N** proceeded normally to afford active HydA1. We then employed pulse EPR spectroscopy to test whether the adt ligand is labeled. The hyperfine coupling to the ^{15}N in adt has been investigated by hyperfine sublevel correlation (HYSCORE) spectroscopy, which revealed a hyperfine tensor of A ^{15}N = [1.9, 1.6, 1,6] MHz (42). The hyperfine values of the 2 ^{13}C carbons, while not previously reported, may be estimated to be comparable to or larger than the ^{15}N hyperfine values, because ^{13}C has larger nuclear g_n value, and they are closer to the spin center. Alternatively, they may be comparable to the ^{13}C hyperfine value of the C9 C in the paramagnetic intermediate found in the C–S bond-forming biotin synthase BioB (a_{iso} = 2.7 MHz), in which the C is located at a similar relative geometry to the diiron cluster as the H-cluster

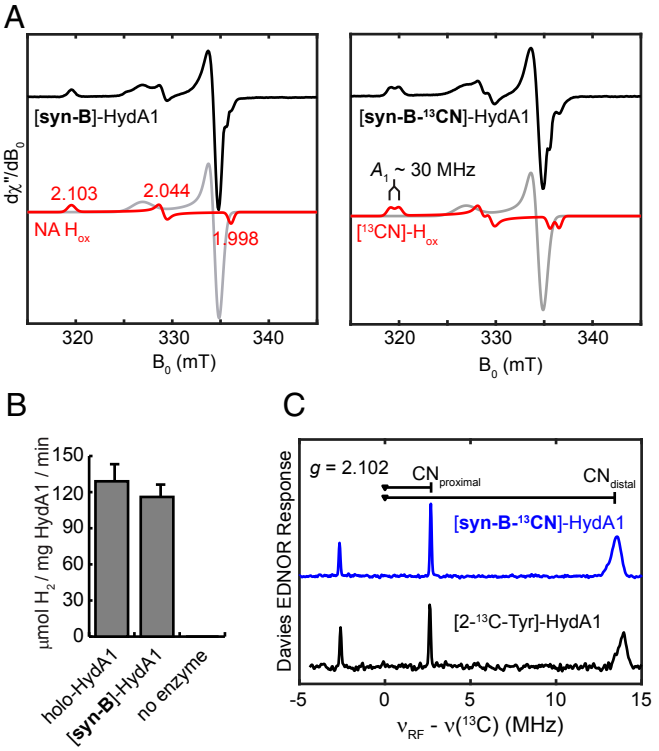

Fig. 3. Characterization of *Cr*HydA1 maturated with **syn-B**. (*A*) X-band CW EPR spectra of [**syn-B**]-*Cr*HydA1 (*Left*) and [**syn-B-^{13}CN**]-*Cr*HydA1 (*Right*). Both spectra were simulated with 2 components: H_{ox}, shown in red traces, and H_{ox}-CO, in gray traces. Conditions were as follows: temperature, 30 K; microwave power, 0.05 mW. (*B*) H_2 evolution activity of [**syn-B**]-*Cr*HydA1 and a holo-*Cr*HydA1 standard measured at 20 °C. (*C*) Q-band Davies ENDOR spectrum of [**syn-B-^{13}CN**]-*Cr*HydA1 H_{ox} and [2-^{13}C-Tyr]-*Cr*HydA1 H_{ox} recorded at g = 2.102 (g_1 of H_{ox}). Conditions were as follows: frequency = 34.1 GHz; temperature = 15 K; inversion pulse = 80 ns; τ = 300 ns; radiofrequency pulse = 20 μs.

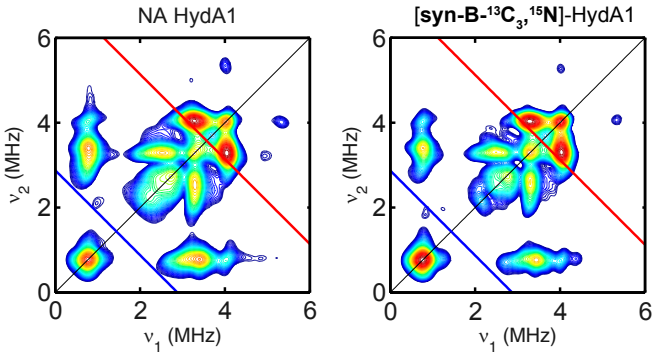

Fig. 4. Comparison of X-band HYSCORE spectra of a *Cr*HydA1 and *Cr*HydA1 maturated from **syn-B-$^{13}C_3$,^{15}N** collected at $g = 2.102$ (g_1 of H_{ox}). The Larmor frequencies of ^{13}C and ^{15}N are indicated in both spectra by red and blue lines, respectively. Conditions were as follows: frequency = 9.8 GHz; temperature = 15 K; τ = 140 ns; $\pi/2$ pulse = 12 ns.

(43). In any case, both ^{13}C and ^{15}N hyperfine couplings should be readily resolved in X-band HYSCORE spectrum. Clearly, however, the HYSCORE spectrum of HydA1 maturated from **syn-B-$^{13}C_3$,^{15}N** exhibited exactly the same patterns as natural abundance HydA1 (Fig. 4) and can be simulated (*SI Appendix*, Fig. S8) by using the ^{14}N hyperfine tensors from the adt and the distal CN ligand, as reported (42). This result indicates that while **syn-B-$^{13}C_3$,^{15}N** results in maturation as expected, the C_2N portion of adt is not labeled, and therefore is not derived from Cys activated in HydG. Additionally, we also added the $^{13}C_3$, ^{15}N-Cys into the maturation reaction directly and didn't find labeled adt ligand either (*SI Appendix*, Fig. S9), indicating that the C and N in adt are indeed not sourced from Cys.

Preparation of HydA1 with **syn-B-$^{13}C_3$,^{15}N** also allows the determination of the fate of the cysteine backbone. Reaction mixtures of maturations using **syn-B** and **syn-B-$^{13}C_3$,^{15}N** were each analyzed for pyruvate and $^{13}C_3$-pyruvate [$^{13}CH_3{}^{13}C(O){}^{13}CO_2^-$] by gas chromatography (GC)-MS (following derivatization; see *SI Appendix* for details). Inspection of the results shows a large background level of pyruvate for both maturations (Scheme 2); however, for the **syn-B-$^{13}C_3$,^{15}N** maturation, $^{13}C_3$-pyruvate was readily distinguished from the unlabeled pyruvate not sourced from **syn-B-$^{13}C_3$,^{15}N**. The maturation reaction using **syn-B-$^{13}C_3$,^{15}N** was found to contain 30 μM $^{13}C_3$-pyruvate, corresponding to approximately twice the concentration of apo-HydA1 used for the maturation. The fact that Cys was converted into pyruvate reinforces our hypothesis that Cys serves only as a source of S for the construction of adt.

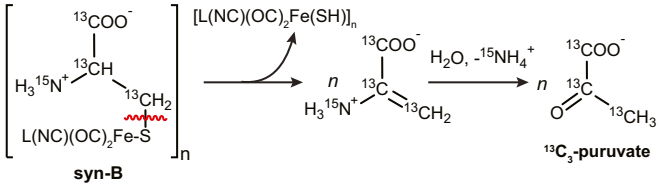

	[pyruvate] (μM)	[$^{13}C_3$-pyruvate] (μM)
Using **syn-B**	366	1.5
Using **syn-B-$^{13}C_3$,^{15}N**	478	30

Scheme 2. Proposed origin of $^{13}C_3$-pyruvate from maturation using **syn-B-$^{13}C_3$,^{15}N** (*Upper*) along with quantification of pyruvate in **syn-B** and **syn-B-$^{13}C_3$,^{15}N** maturation reactions (*Lower*). L, unspecified labile ligand.

Maturation of Apo-HydA1 with Syn-B-Secys Gives the Seleno-adt Derivative. To further establish that Cys serves as a S donor, experiments were conducted to demonstrate that selenocysteine serves as a Se donor. The required carrier **syn-B-Secys** was prepared completely analogously to the preparation of **syn-B** by reaction of selenocysteine and $[FeI_2(CN)(CO)_3]^-$. In terms of its ESI-MS and FT-IR properties, **syn-B-Secys** and **syn-B** are very similar (*SI Appendix*, Fig. S5 and Table S1). Maturation with **syn-B-Secys** gave *Cr*HydA1-Se, whose EPR spectrum was virtually indistinguishable from native *Cr*HydA1, except some broadening at g_1 (*SI Appendix*, Fig. S10). Incorporation of Se into HydA1-Se was definitively characterized with EXAFS, both at the Se and Fe edges (44). The Se K EXAFS and FT are shown in Fig. 5, with simulated metrical parameters listed in *SI Appendix*, Table S2. The data simulated well to 2 Se–Fe interactions with Se–Fe = 2.43 Å and a Debye–Waller (DW) term of 0.0065 Å^2. The value of the DW factor is similar to that obtained for a SeCys ligand bridging between 2 Cu(I) centers in SeCys-labeled Cu(I)-CCS (45) and is consistent with the Se atom bridging between 2 Fe atoms of the subcluster. The Se data do not permit the number of Se bridges to be determined, but if the Se is incorporated into the adt ligand, the expectation is that 2 such bridges will be present. To gain insight, we also analyzed the Fe K EXAFS of the S- and Se-containing HydA1 systems, which are shown for comparison in *SI Appendix*, Figs. S11 and S12. Although these spectra are similar, there are clear differences which can be accounted for by inclusion of Fe–Se scattering in the SeCys derivative. Importantly, the best fits to the Fe data were obtained when 2 Fe–Se scatterers per Fe atom of the $[2Fe]_H$ subcluster were included with identical Fe–Se distances and DW factors as determined at the Se edge. Thus, we conclude that our data are supportive of an HydA1 subcluster containing 2 bridging Se-containing ligands, as expected for an Se–adt interaction. To summarize, these results reveal the fate of Cys during the H-cluster bioassembly as donating the S atom to the adt ligand with its backbone converted into pyruvate, as depicted in Scheme 3.

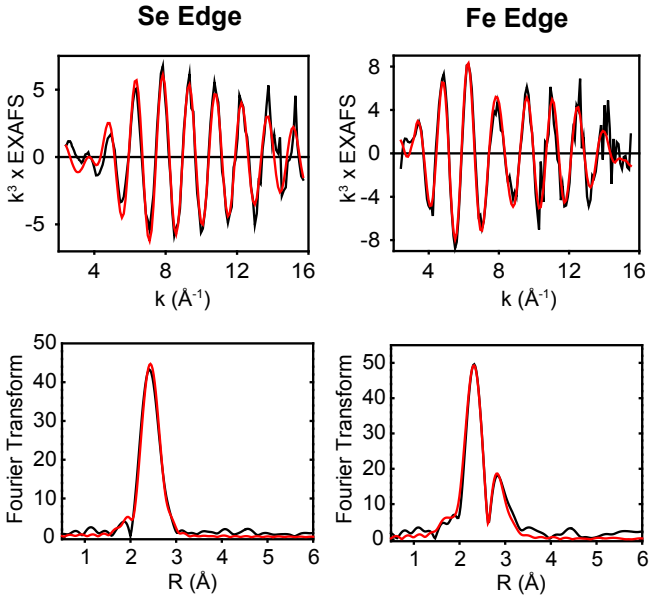

Fig. 5. Se K-edge (*Left*) and Fe K-edge (*Right*) EXAFS (*Upper*) and the corresponding Fourier transforms (*Lower*) of the Se-labeled *Cr*HydA1. Black traces are experimental data and red traces are simulations using the parameters listed in *SI Appendix*, Table S2.

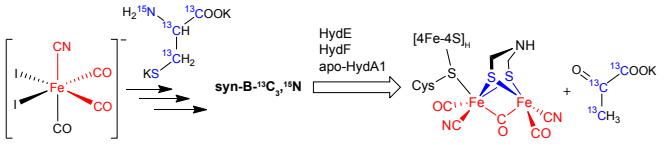

Scheme 3. Summary and implications of maturation with **syn-B-$^{13}C_3$, ^{15}N**: HydG produces the precursor to the $Fe_2S_2(CN)_2(CO)_3$ portion of HydA1.

Discussion

A combination of synthetic organometallic chemistry, biochemical techniques, and biophysical analyses provides unique insights into the biosynthesis of the catalytic center of the [FeFe] hydrogenase. The synthetic surrogate **syn-B** is a fully functional analog of Complex B, the proposed product of the radical SAM maturase enzyme HydG. Because it is far more robust than Complex B, **syn-B** has allowed us to eliminate HydG in the in vitro maturation protocol. While the exact composition of **syn-B** in not fully understood, FT-IR, ESI-MS, and elemental analyses confirmed that it contains the targeted $[Fe(Cys)(CN)(CO)_2]$ fragment, which has been postulated to be the essential component of Complex B.

Regardless of the precise structure of **syn-B**, this surrogate allows us to gain major insights into the biosynthesis of the H-cluster of [FeFe] hydrogenase. With the added control associated with **syn-B**, we were able to selectively test the effects on maturation by sequentially replacing cysteine with cysteamine (lacking the carboxylate). The inability of **syn-B-cysam** to form maturated HydA1 indicates that cysteine is necessary for maturation. Furthermore, the finding that mixtures of **syn-B-cysam** and Cys do not maturate implies that **syn-B**, and logically, Complex B, is a source, not only of the diatomic ligands but of $Fe(CN)(CO)_2S$. These findings imply that the $Fe(CN)(CO)_2(Cys)$ is a cohesive module. Such behavior is consistent with its being a low-spin d^6 center, which confers kinetic robustness to this module.

This strategy also allows for isotopic labeling of the cysteine in the maturation, which has not been possible with typical maturation using HydG because protocols do not exist for replacing auxiliary Fe–S cluster-ligated natural abundance cysteine with labeled cysteine or selenocysteine. Maturation with **syn-B-$^{13}C_3$, ^{15}N** was successful; however, no ^{13}C or ^{15}N appeared to incorporate into the adt of the final HydA1 produced. This result is surprising: It shows that Complex B is not the source of C or N for adt formation. Instead, the Cys backbone is found to convert into pyruvate. Consistent with these results, maturation with **syn-B-Se** results in the incorporation of Se into the H-cluster. These results clearly indicate that Cys only donates its S atom to the H-cluster. Given that in HydG, the cysteine ligand stabilizes the dangler Fe relative to its highly labile form without cysteine (26, 34), it is interesting to observe that the Fe–S bond remains intact in the formation of the Fe_2S_2 core of the binuclear subcluster.

This work sets the stage for other studies involving the preparation of modified and isotopically labeled versions of Complex B. We have shown that this synthetic surrogate strategy is a fruitful venture that powerfully complements biochemical strategies aimed at understanding pathways involved in the maturation of [FeFe]-hydrogenase. Future work will focus on synthesizing more well-defined surrogates for Complex B, while also developing new complexes incorporating other ligands to identify the source of C and N for adt formation. The abstraction of S from cysteine is reminiscent of the Fe–S cluster biogenesis system (the *isc* operon) employed for the biosynthesis of ferredoxins (46), except that S transfer affords pyruvate, not alanine. This indicates interesting C–S bond cleavage and formation reaction(s) mediated probably by HydE or HydF. In the future, as prospective products of HydE and HydF are hypothesized, this surrogate strategy will likely be useful in investigating the molecular mechanism of these enzymes and identifying intermediates at later stages in the maturation pathway.

Materials and Methods

Synthetic organometallic chemistry leading to **syn-B**, **syn-B-^{13}CN**, **syn-B-$^{13}C_3$, ^{15}N**, **syn-B-cysam**, and **syn-B-Secys** were conducted by using glovebox and Schlenkline techniques. Maturation experiments followed recently published protocols (37, 47). Additional details together with spectra and simulation details can be found in *SI Appendix*.

ACKNOWLEDGMENTS. This work was supported by NIH Grants 1R35GM126961-01 (to R.D.B.), GM61153 (to T.B.R.), and R01GM123725 (to N.J.B.). Use of the Stanford Synchrotron Radiation Lightsource, SLAC National Accelerator Laboratory, is supported by the US Department of Energy (DOE), Office of Science, Office of Basic Energy Sciences Contract DE-AC02-76SF00515. The Stanford Synchrotron Radiation Lightsource Structural Molecular Biology Program is supported by the DOE Office of Biological and Environmental Research and by the National Institutes of Health, National Institute of General Medical Sciences (including Grant P41 GM103393). We thank Prof. Frank E. Osterloh and Dr. Zeqiong Zhao (University of California, Davis) for the help with GC detection of H_2; and Dr. Lucas Li and Dr. Alexander Ulanov at the Roy J. Carver Biotechnology Center (University of Illinois Urbana–Champaign) for help with pyruvate detection and quantification.

1. W. Lubitz, H. Ogata, O. Rüdiger, E. Reijerse, Hydrogenases. *Chem. Rev.* **114**, 4081–4148 (2014).
2. K. Pandey, S. T. Islam, T. Happe, F. A. Armstrong, Frequency and potential dependence of reversible electrocatalytic hydrogen interconversion by [FeFe]-hydrogenases. *Proc. Natl. Acad. Sci. U.S.A.* **114**, 3843–3848 (2017).
3. R. M. Evans *et al.*, The value of enzymes in solar fuels research—Efficient electrocatalysts through evolution. *Chem. Soc. Rev.* **48**, 2039–2052 (2019).
4. D. W. Mulder, Y. Guo, M. W. Ratzloff, P. W. King, Identification of a catalytic iron-hydride at the H-cluster of [FeFe]-hydrogenase. *J. Am. Chem. Soc.* **139**, 83–86 (2017).
5. V. Pelmenschikov *et al.*, Reaction coordinate leading to H_2 production in [FeFe]-hydrogenase identified by nuclear resonance vibrational spectroscopy and density functional theory. *J. Am. Chem. Soc.* **139**, 16894–16902 (2017).
6. E. J. Reijerse *et al.*, Direct observation of an iron-bound terminal hydride in [FeFe]-hydrogenase by nuclear resonance vibrational spectroscopy. *J. Am. Chem. Soc.* **139**, 4306–4309 (2017).
7. C. Sommer *et al.*, Proton coupled electronic rearrangement within the H-cluster as an essential step in the catalytic cycle of [FeFe] hydrogenases. *J. Am. Chem. Soc.* **139**, 1440–1443 (2017).
8. E. M. Shepard *et al.*, [FeFe]-hydrogenase maturation. *Biochemistry* **53**, 4090–4104 (2014).
9. J. N. Betz *et al.*, [FeFe]-hydrogenase maturation: Insights into the role HydE plays in dithiomethylamine biosynthesis. *Biochemistry* **54**, 1807–1818 (2015).
10. J. B. Broderick *et al.*, H-cluster assembly during maturation of the [FeFe]-hydrogenase. *J. Biol. Inorg. Chem.* **19**, 747–757 (2014).
11. D. W. Mulder *et al.*, Insights into [FeFe]-hydrogenase structure, mechanism, and maturation. *Structure* **19**, 1038–1052 (2011).
12. J. W. Peters *et al.*, [FeFe]- and [NiFe]-hydrogenase diversity, mechanism, and maturation. *Biochim. Biophys. Acta* **1853**, 1350–1369 (2015).
13. G. Berggren *et al.*, Biomimetic assembly and activation of [FeFe]-hydrogenases. *Nature* **499**, 66–69 (2013).
14. D. W. Mulder *et al.*, Stepwise [FeFe]-hydrogenase H-cluster assembly revealed in the structure of $HydA^{\Delta EFG}$. *Nature* **465**, 248–251 (2010).
15. S. E. McGlynn *et al.*, HydF as a scaffold protein in [FeFe] hydrogenase H-cluster biosynthesis. *FEBS Lett.* **582**, 2183–2187 (2008).
16. E. M. Shepard *et al.*, Synthesis of the 2Fe subcluster of the [FeFe]-hydrogenase H cluster on the HydF scaffold. *Proc. Natl. Acad. Sci. U.S.A.* **107**, 10448–10453 (2010).
17. P. Berto *et al.*, The [4Fe-4S]-cluster coordination of [FeFe]-hydrogenase maturation protein HydF as revealed by EPR and HYSCORE spectroscopies. *Biochim. Biophys. Acta* **1817**, 2149–2157 (2012).
18. G. Caserta *et al.*, Structural and functional characterization of the hydrogenase-maturation HydF protein. *Nat. Chem. Biol.* **13**, 779–784 (2017).
19. R. Rohac *et al.*, Carbon-sulfur bond-forming reaction catalysed by the radical SAM enzyme HydE. *Nat. Chem.* **8**, 491–500 (2016).
20. J. M. Kuchenreuther *et al.*, A radical intermediate in tyrosine scission to the CO and CN^- ligands of FeFe hydrogenase. *Science* **342**, 472–475 (2013).
21. E. Pilet *et al.*, The role of the maturase HydG in [FeFe]-hydrogenase active site synthesis and assembly. *FEBS Lett.* **583**, 506–511 (2009).
22. E. M. Shepard *et al.*, [FeFe]-hydrogenase maturation: HydG-catalyzed synthesis of carbon monoxide. *J. Am. Chem. Soc.* **132**, 9247–9249 (2010).
23. R. C. Driesener *et al.*, Biochemical and kinetic characterization of radical S-adenosyl-L-methionine enzyme HydG. *Biochemistry* **52**, 8696–8707 (2013).
24. A. Pagnier, L. Martin, L. Zeppieri, Y. Nicolet, J. C. Fontecilla-Camps, CO and CN^- syntheses by [FeFe]-hydrogenase maturase HydG are catalytically differentiated events. *Proc. Natl. Acad. Sci. U.S.A.* **113**, 104–109 (2016).

25. J. M. Kuchenreuther *et al*., The HydG enzyme generates an $Fe(CO)_2(CN)$ synthon in assembly of the FeFe hydrogenase H-cluster. *Science* **343**, 424–427 (2014).
26. P. Dinis *et al*., X-ray crystallographic and EPR spectroscopic analysis of HydG, a maturase in [FeFe]-hydrogenase H-cluster assembly. *Proc. Natl. Acad. Sci. U.S.A.* **112**, 1362–1367 (2015).
27. D. L. Suess, J. M. Kuchenreuther, L. De La Paz, J. R. Swartz, R. D. Britt, Biosynthesis of the [FeFe] hydrogenase H cluster: A central role for the radical SAM enzyme HydG. *Inorg. Chem.* **55**, 478–487 (2016).
28. D. L. Suess *et al*., The radical SAM enzyme HydG requires cysteine and a dangler iron for generating an organometallic precursor to the [FeFe]-hydrogenase H-cluster. *J. Am. Chem. Soc.* **138**, 1146–1149 (2016).
29. G. Rao, L. Tao, D. L. M. Suess, R. D. Britt, A [4Fe-4S]-Fe(CO)(CN)-L-cysteine intermediate is the first organometallic precursor in [FeFe] hydrogenase H-cluster bioassembly. *Nat. Chem.* **10**, 555–560 (2018).
30. A. Stock *et al*., Synthesis of fac-$[Fe^{II}(CN)(CO)_3I_2]^-$ and chemistry of the fac-$[Fe^{II}(CN)_x(CO)_3I_{(3-x)}]^-$ series (x=1–3). *Inorg. Chem. Commun.* **18**, 105–109 (2012).
31. W. F. Liaw *et al*., Dinuclear iron(II)-cyanocarbonyl complexes linked by two/three bridging ethylthiolates: Relevance to the active site of [Fe] hydrogenases. *Inorg. Chem.* **42**, 2783–2788 (2003).
32. C.-H. Chen *et al*., Preparative and structural studies on iron(II)-thiolate cyanocarbonyls: Relevance to the [NiFe]/[Fe]-hydrogenases. *Dalton Trans.*, 137–143 (2004).
33. C. H. Lai *et al*., Responses of the $Fe(CN)_2(CO)$ unit to electronic changes as related to its role in [NiFe]hydrogenase. *J. Am. Chem. Soc.* **120**, 10103–10114 (1998).
34. D. L. Suess *et al*., Cysteine as a ligand platform in the biosynthesis of the FeFe hydrogenase H cluster. *Proc. Natl. Acad. Sci. U.S.A.* **112**, 11455–11460 (2015).
35. V. E. Kaasjager *et al*., A structural model for [Fe]-only hydrogenases. *Angew. Chem. Int. Ed. Engl.* **37**, 1668–1670 (1998).
36. P. I. Volkers *et al*., Precursors to [FeFe]-hydrogenase models: Syntheses of $Fe_2(SR)_2(CO)_6$ from CO-free iron sources. *Inorg. Chem.* **47**, 7002–7008 (2008).
37. G. Rao, R. D. Britt, Electronic structure of two catalytic states of the [FeFe] hydrogenase H-cluster as probed by pulse electron paramagnetic resonance spectroscopy. *Inorg. Chem.* **57**, 10935–10944 (2018).
38. J. M. Kuchenreuther, S. J. George, C. S. Grady-Smith, S. P. Cramer, J. R. Swartz, Cell-free H-cluster synthesis and [FeFe] hydrogenase activation: All five CO and CN^- ligands derive from tyrosine. *PLoS One* **6**, e20346 (2011).
39. W. K. Myers *et al*., The cyanide ligands of [FeFe] hydrogenase: Pulse EPR studies of ^{13}C and ^{15}N-labeled H-cluster. *J. Am. Chem. Soc.* **136**, 12237–12240 (2014).
40. R. Angamuthu *et al*., N-substituted derivatives of the azadithiolate cofactor from the [FeFe] hydrogenases: Stability and complexation. *Inorg. Chem.* **54**, 5717–5724 (2015).
41. J. E. Cronan, Advances in synthesis of biotin and assembly of lipoic acid. *Curr. Opin. Chem. Biol.* **47**, 60–66 (2018).
42. A. Adamska-Venkatesh *et al*., Spectroscopic characterization of the bridging amine in the active site of [FeFe] hydrogenase using isotopologues of the H-cluster. *J. Am. Chem. Soc.* **137**, 12744–12747 (2015).
43. L. Tao, T. A. Stich, C. J. Fugate, J. T. Jarrett, R. D. Britt, EPR-derived structure of a paramagnetic intermediate generated by biotin synthase BioB. *J. Am. Chem. Soc.* **140**, 12947–12963 (2018).
44. L. Kertess *et al*., Chalcogenide substitution in the [2Fe] cluster of [FeFe]-hydrogenases conserves high enzymatic activity. *Dalton Trans.* **46**, 16947–16958 (2017).
45. A. N. Barry, N. J. Blackburn, A selenocysteine variant of the human copper chaperone for superoxide dismutase. A Se-XAS probe of cluster composition at the domain 3-domain 3 dimer interface. *Biochemistry* **47**, 4916–4928 (2008).
46. R. Lill, Function and biogenesis of iron-sulphur proteins. *Nature* **460**, 831–838 (2009).
47. J. M. Kuchenreuther, S. A. Shiigi, J. R. Swartz, Cell-free synthesis of the H-cluster: A model for the in vitro assembly of metalloprotein metal centers. *Methods Mol. Biol.* **1122**, 49–72 (2014).